

# The Role of Jiningian Pluton in Yanshanian Metallogenic Events in the Dahutang Tungsten Deposit: Evidence from Whole Rock and Zircon Geochemistry

Guofeng Xu <sup>1</sup>, Zhenyu Li <sup>1</sup>, Xiaoyong Yang <sup>2</sup> and Lei Liu <sup>1,\*</sup>

<sup>1</sup> Key Laboratory of Metallogenic Prediction of Nonferrous Metals and Geological Environment Monitoring, Ministry of Education, School of Geosciences and Info-Physics, Central South University, Changsha 410083, China; 215011007@csu.edu.cn (G.X.); 8208190317@csu.edu.cn (Z.L.)

<sup>2</sup> CAS Key Laboratory of Crust-Mantle Materials and Environments, School of Earth and Space Sciences, University of Science and Technology of China, Hefei 230026, China; xxyang@ustc.edu.cn

\* Correspondence: liu01@ustc.edu.cn; Tel.: +86-731-8883-0616

**Abstract:** The Dahutang tungsten deposit is one of the largest deposits in the Jiangnan tungsten belt. The Jiningian pluton is widely distributed in the orefield, which is considered an ore-bearing wall rock and Ca source for scheelite mineralization. The Jiningian granodiorite samples near ore have high W contents (average 93 ppm). Moreover, their SiO<sub>2</sub> and P<sub>2</sub>O<sub>5</sub> contents are positively correlated in Harker diagrams, and the A/CNK values vary between 1.18–1.71, suggesting that the Jiningian granodiorite is high fractionated S-type granites and has the potential for W mineralization. The zircon U-Pb ages of the Jiningian granodiorite samples (17SWD-1, 17SWD-2) are 845 ± 21 Ma (MSWD = 1.7) and 828.7 ± 7.5 Ma (MSWD = 1.0), respectively, representing the formation ages of the Jiningian pluton. The U-Pb age of hydrothermal zircons (~140 Ma) in the Jiningian granodiorite samples is consistent with the mineralization age (150–139 Ma), indicating the strong superimposed modification of the Yanshanian mineralizing fluids. The positive correlation between Ca and W molarity in the Jiningian granodiorite samples demonstrates that they provide considerable Ca and W during Yanshanian mineralization. The W activation migration due to sodium alteration can be inferred from the inverse correlation between Na and W molarity. The study tries to provide a new perspective on the origin of mineralized material in the world-class Dahutang tungsten deposit.

**Keywords:** Dahutang tungsten deposit; Jiningian pluton; Yanshanian ore bodies; superimposed mineralization; hydrothermal modification

**Citation:** Xu, G.; Li, Z.; Yang, X.; Liu, L. The Role of Jiningian Pluton in Yanshanian Metallogenic Events in the Dahutang Tungsten Deposit: Evidence from Whole Rock and Zircon Geochemistry. *Minerals* **2022**, *12*, 428. <https://doi.org/10.3390/min12040428>

Academic Editor: Paul Alexandre

Received: 28 February 2022

Accepted: 28 March 2022

Published: 30 March 2022

**Publisher's Note:** MDPI stays neutral with regard to jurisdictional claims in published maps and institutional affiliations.



**Copyright:** © 2022 by the authors. Licensee MDPI, Basel, Switzerland. This article is an open access article distributed under the terms and conditions of the Creative Commons Attribution (CC BY) license (<https://creativecommons.org/licenses/by/4.0/>).

## 1. Introduction

South China is one of the largest tungsten mineralization provinces in the world, with several large and ultra-large tungsten deposits, especially in the Nanling region [1,2]. However, in recent years, a number of porphyry-skarn tungsten deposits have been discovered and identified in Jiangnan Massif and its adjacent areas, which constitutes a tungsten belt called the Jiangnan tungsten belt [3,4]. The proven tungsten resources in this belt amount to nearly 6.06 Mt, among which the typical deposit of Dahutang has reached 1.07 Mt of tungsten resources [5,6]. The source of such a huge amount of tungsten resources and its enrichment mechanism have become the focus of geologists.

Previous studies have suggested that Yanshanian granite is the parent rock of the Dahutang tungsten deposit. The evidence for this is mainly the following four points: (1) The diagenetic age of Yanshanian granites (153–134 Ma) is more in agreement with the mineralization age (150–139 Ma, [3,5,7–14]); (2) The source area of the Yanshanian rocks is the shallow metamorphic rocks of the Shuangqiaoshan Group, which is a high background area for W, with a 3.23-times higher tungsten content than the crustal Clark value

[15,16]; (3) The tungsten content of Yanshanian rocks is 10–100 times higher than the crust [3,7,17,18]; (4) The Yanshanian rocks are highly differentiated S-type granites, which is closely related to the formation of tungsten ore [8]. For the Jiningian rocks in the region, previous work has considered them as a source of Ca for scheelite ( $\text{CaWO}_4$ ) during the Yanshanian mineralization event based on their large size and high Ca content [7,19,20]. However, Sr-Nd isotopic characteristics show that the source area of Jiningian rocks is also the shallow metamorphic rocks of the Shuangqiaoshan Group [20,21]. They are highly differentiated S-type granites and have tungsten content 9.5 times higher than the crustal Clark value [16,21]. Moreover, as ore-bearing wall-rocks, the Jiningian rocks have close contact with the ore body, which implies that they contributed part of the mineralized material [3]. Unfortunately, the few scholars who have noticed this problem do not give direct evidence [9,22]. Moreover, how the Jiningian rocks provide mineralized material is unclear. Therefore, finding out the relationship between tungsten mineralization and the Jiningian pluton is significant to understanding the source and formation mechanism of these large tungsten deposits.

In this study, whole-rock major and trace element, zircon CL imaging, LA-ICP-MS U-Pb dating and trace element studies have been carried out on the near-mine Jiningian granodiorite of the Dahutang deposit. This study is expected to confirm that the Jiningian rocks contributed mineralized material during the Yanshanian mineralization event, clarify the mechanism of this process and provide new insights into the genesis of world-class W deposits in the Jiangnan tungsten belt.

## 2. Regional and Deposit Geology

The Dahutang porphyry W deposit is located in the western region of the Jiangnan tungsten belt, south of the Middle–lower Yangtze River belt. On the northern margin of the Yangtze craton, the Middle–lower Yangtze River belt is located along the middle and lower Yangtze River basin (Figure 1a). The Xiangfan-Guangji and Tancheng-Lujiang faults, which separate the belt from the Dabie orogenic band and the North China Craton, respectively, mark its northern and western boundaries [23]. The Yang-xing-Changzhou fault zones form the southern boundary of the belt and separate it from the rest of the Yangtze Craton, which includes the Jiangnan Massif [24]. The Jiangnan tungsten belt lies south of the Middle–lower Yangtze River belt and extends mainly along the Jiangnan Massif and its eastern foothills. The strata exposed in Jiangnan Massif and adjacent areas are Precambrian basement and Phanerozoic cover [4,25,26]. The Neoproterozoic Shuangqiaoshan Group strata are mainly diorite and metavolcanic sedimentary rocks, and their age (~830 Ma) represents the formation age of the Jiangnan orogenic belt [27,28]. Since the Neoproterozoic, it has experienced many tectonic movements, such as the Jining, Garidon, Haixi, Indochinese and Yanshan periods, and large-scale fold and overthrust structures, fracture zones and ductile shear zones have developed in the area [1,29,30].

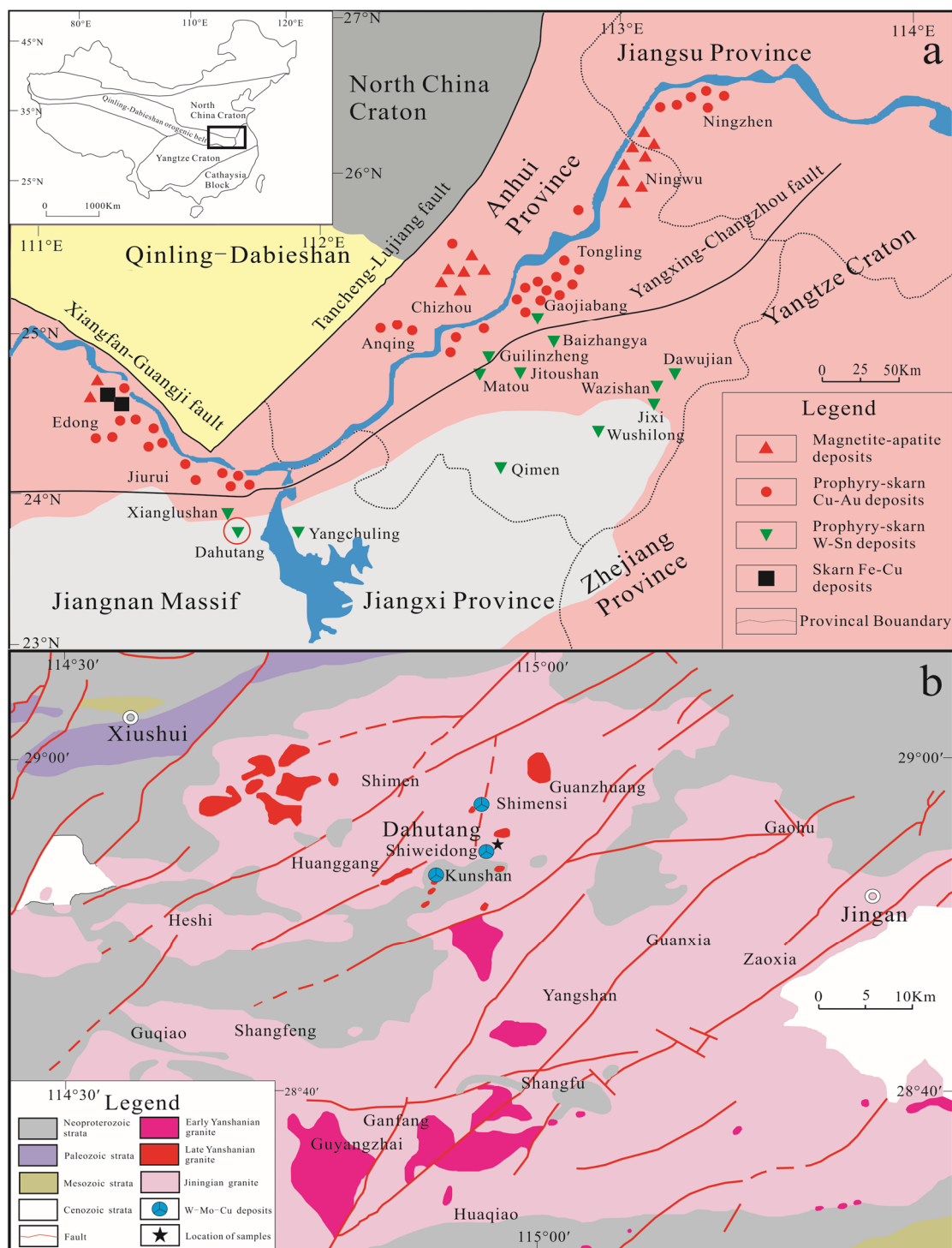


**Figure 1.** (a) Distribution of ore clusters (districts) in the Middle and Lower Yangtze River metallogenic belt and deposits in the Jiangnan tungsten belt (the insert shows the general tectonic divisions of China, the black rectangle indicates the position of Figure 1a and the circled triangle represent the location of the Dahutang deposit.) (modified after [5]); (b) Sketch geological map of the Dahutang tungsten polymetallic mine region and the surrounding area in northwestern Jiangxi Province, South China (modified after [31]).

In recent years, many tungsten deposits have been discovered in the Jiangnan Massif and its neighboring area [4]. So far, the proven tungsten resources in the Jiangnan tungsten belt are nearly 6.06 Mt, of which 1.07 Mt are in Dahutang [4,6]. The Dahutang tungsten deposit is located in the northwestern part of Jiangxi Province, at the junction of Wuning, Xiushui and Jingan counties (Figure 1b). The mine region mostly exposes

Neoproterozoic Shuangqiaoshan Group shallow metamorphic rocks that are heavily laminated, with a general north-east orientation and a south–south-east trend, with a dip angle of 60° to 80° [3,32,33]. The granite group in the mine region is very well developed and consists mainly of Neoproterozoic granodiorite and Early Cretaceous granite [5]. The former is produced as a base, and the latter is produced as a small strain, tuber or wall (vein) [19]. The Yanshan-age igneous rocks of the Dahutang tungsten deposit are characterized by a multi-phase intrusion, including medium and fine-grained biotite granite, porphyritic muscovite granite and a small amount of granite porphyry [3,19,32,33]. They intruded the Neoproterozoic granodiorite body and developed strong tungsten mineralization in the inner–outer contact zone [19]. The mineralization type of the Dahutang deposit is mainly fine-vein dipping scheelite (wolframite) where scheelite and wolframite co-exist, accompanied by other types of quartz vein, altered granite, greisen and hydrothermal breccia [10,12,13]. The Jiningian pluton, which mainly consists of granodiorite, is part of the Jiuling batholith. It occurs throughout the mine region and is in close contact with the ore body (Figure 1b). Under the microscope, minerals such as quartz, biotite, potassium feldspar and andesine can be seen, as well as albite and sericitic alteration (Figure 2). The quartz is semi-automorphic, with a grain size of about 0.5 mm, accounting for about 50% of the total rock (Figure 2). The biotite is flaky and has a high interference color, accounting for about 10% of the total rock. The K-feldspar is approximately 1 mm in grain size, where significant sericitization occurs (Figure 2d). The albite is characterized by polysynthetic twin, mostly around the potassium feldspar (Figure 2c–f). Andesine is characterized by weak ring banding and has a larger grain size of up to 2 mm (Figure 2g,h).

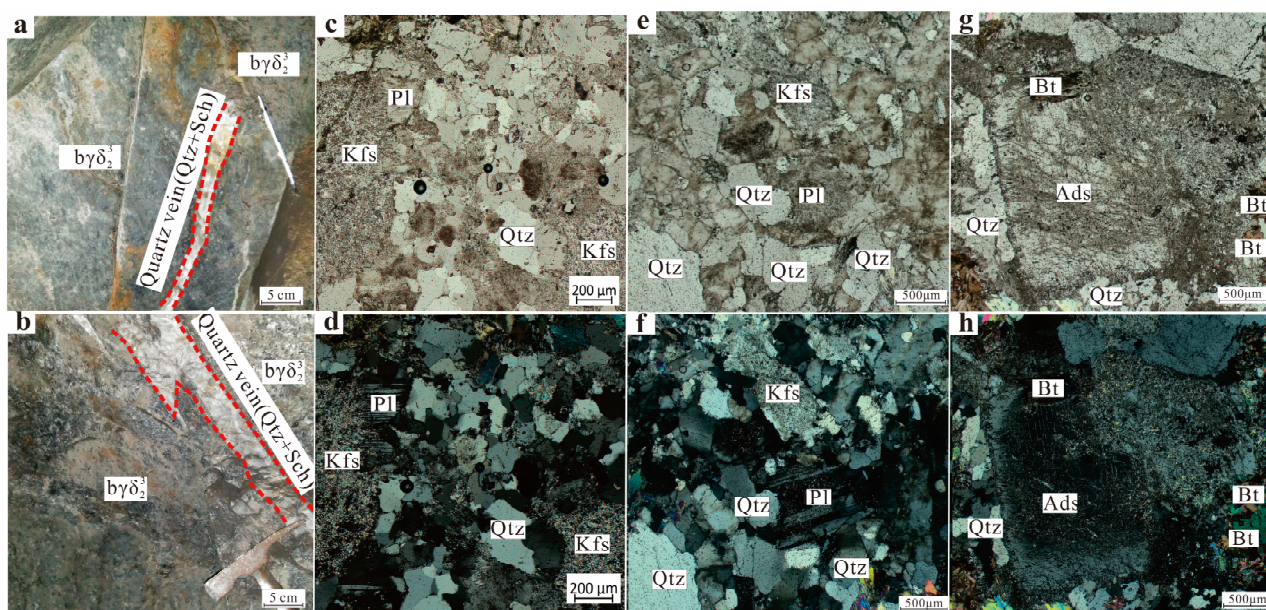


**Figure 2.** Field (a,b) and microscopic photos (c–h) of Jiningian granodiorite in the Dahutang deposit. by $\delta_2$ : Jiningian granodiorite; Sch: scheelite; Qtz: quartz; Pl: plagioclase; Kfs: K-feldspar; Bt: biotite; Ads: andesine.

### 3. Sampling and Analytical Techniques

After conducting a detailed geological survey of the Dahutang porphyry W deposit, we collected typical samples of the Jiningian pluton located near the scheelite ore body from the Shiweidong mine of the Dahutang deposit. Then, LA-ICP-MS zircon U-Pb dating, whole-rock major and trace element analysis and zircon trace elements determinations were performed on the Jiningian granodiorite samples.

### 3.1. Major and Trace Elements

The testing of whole-rock major and trace elements was completed at the Guangzhou Aoshi Mineral Laboratory (Guangzhou, China). Whole-rock major elements were analyzed by X-ray fluorescence spectrometry. Firstly, the granodiorite samples collected in the field were crushed and ground to 200 mesh indoors to obtain powder samples. Then, three samples were weighed. One sample was acid-dried, dissolved and fixed, and the S-Ca-Fe-Mn-Cr content was measured roughly using an Agilent 5001 ICP-AES. The second specimen is dried, weighed accurately, mixed with lithium tetraborate-lithium metaborate-lithium nitrate in a platinum crucible and melted at 1050 °C in a melting machine. The molten slurry was made into molten flakes whose major elements were determined using a PANalytical PW2424 XRF spectrometer. The third specimen was dried and weighed in a certain amount, then aerobically scorched in a muffle furnace at 1000 °C. After cooling, it was accurately weighed, and the mass difference between the two weights was calculated as Loss on Ignition (LOI). The lower limit of detection for major elements is 0.01%, with an error of less than 2%.

Two powder samples were weighed for trace element analysis. One sample was digested with perchloric, nitric and hydrofluoric acid, then evaporated, dissolved, spiked and analyzed by Agilent 5001-type ICP-AES and Agilent7900-type ICP-MS. The other specimen is added to the lithium tetra-borate melt mixed well and melted in a furnace above 1025 °C. After the melt was cooled, we fixed it and analyzed the trace elements by Agilent 7900-type ICP-MS. The final trace element results are based on a combination of the digestion results and the actual conditions of the samples. The error in trace element testing is less than 10%.

### 3.2. Zircon U–Pb Dating and Trace Elements Analyses

Zircon sorting and target making were carried out at Langfang Shangyi Rock and Mineral Testing Technical Services (Langfang city, Hebei province, China). Zircon grains were separated from bulk samples by conventional density and magnetic separation techniques. The representative zircon particles were selected manually under the binocular microscope. The selected zircon grains were embedded in epoxy resin and polished until they were ground to the near central section of zircon crystal, and then the transmitted and reflected light images were taken under the optical microscope.

Zircon U-Pb dating and trace element analyses were carried out at the Key Laboratory for the study of focused Magmatism and Giant ore Deposits, MLR. Xi'an Center of Geological Survey, CGS, Xi'an, China. Before analysis, the cathodoluminescence (CL) image of zircons was obtained by TESCAN MIRA3 Scanning Electron Microscope with Mono CL System in Key Laboratory of Crust-Mantle Materials and Environments, University of Science and Technology of China, Chinese Academy of Sciences. After selecting the analysis points by CL images, using an Agilent 7700× ICP-MS with a GeoLas Pro laser to analyze the uranium to lead ratio in the zircon microregion. Helium is used as the carrier gas to avoid the air wear of the selected single crystal. Each measurement point was analyzed for 50 s, including 10 s of blank signal and 40 s of sample signal. The offline processing of the analysis data is conducted using the software Glitter 4.4 [34]. Detailed instrument parameters and test procedures have been provided by Li et al. (2015) [35]. Zircon standard 91,500 was used as an external standard for isotopic fractionation correction in the U-Pb isotope dating. U-Pb age harmonic mapping and age-weight averaging of zircon samples were conducted using Isoplot/Ex\_ver 3 [36]. Zircon trace element contents were quantified using the reference standard NIST610 glass as a multiple external standard and Si as an internal standard.

## 4. Results

### 4.1. Major and Trace Elements

The present study of Dahutang Jiningian granodiorite has a SiO<sub>2</sub> content of 65.87% to 68.21%. In the TAS diagram, the projection points of seven samples fall in the granite and granodiorite zone in agreement with previous authors (Figure 3). The A/CNK values of the samples range from 1.18 to 1.71, and the subpoints in the diagram of the Al

saturation index all fall within the peraluminous granite zone (Figure 4). In addition, the Hacker diagram shows that  $Al_2O_3$ ,  $MgO$ ,  $CaO$ ,  $TiO_2$  and  $Fe_2O_3T$  show a negative correlation with  $SiO_2$  while  $Na_2O$  and  $K_2O$  have the opposite, which is in high agreement with the previous data (Figure 5a–f,h).  $P_2O_5$  is positively correlated with  $SiO_2$ (Figure 5g), reflecting the characteristics of S-type granites.

The REE contents of Dahutang Jiningian granodiorite range from 74.29 ppm to 162.66 ppm, with an average of 99.48 ppm. Among them,  $\Sigma LREE$  ranges from 61.4 ppm to 141.3 ppm, and  $\Sigma HREE$  ranges from 6.8 to 21.4 ppm, with light rare earths being relatively enriched and heavy rare earths being deficient. Moreover, our samples have significant negative Eu anomalies ( $Eu^* = 0.10\text{--}0.19$ ) and positive Ce anomalies ( $Ce^* = 4.30\text{--}4.49$ ). Major and trace elements results are listed in Supplementary Table S1.

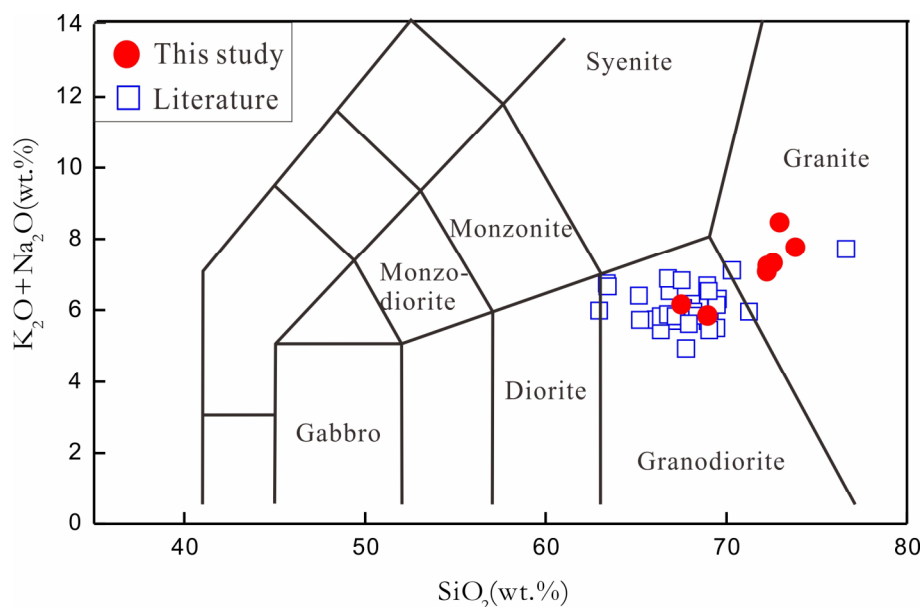


**Figure 3.** TAS diagram of rock classification of Jiningian granodiorite in the Dahutang deposit (modified after [37]). Previous data from [20,21,38,39], as shown in Supplementary Table S2.

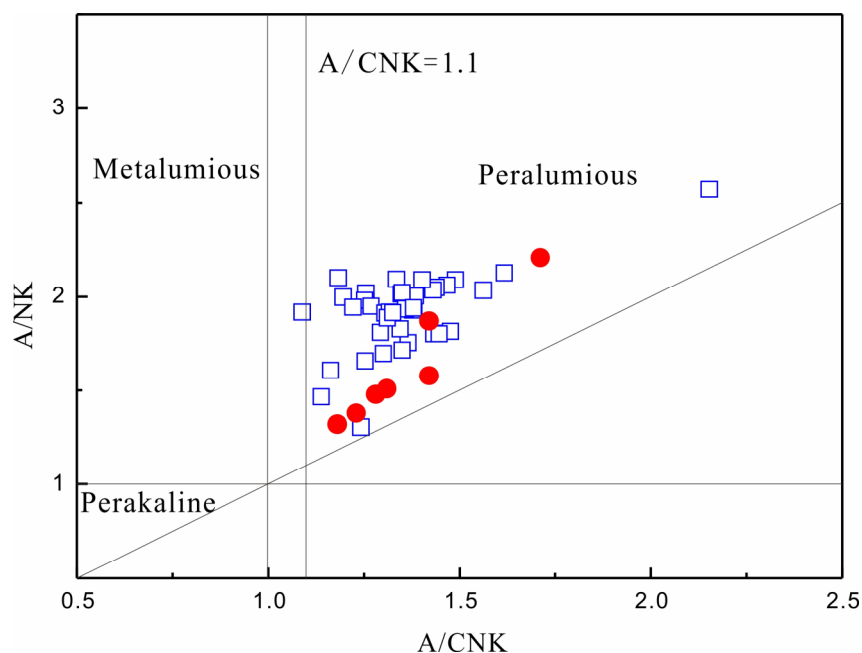


**Figure 4.** Diagram of Al saturation index of Jiningian granodiorite in the Dahutang deposit (modified after [40]). Previous data from [20,21,38,39], as shown in Table S2.

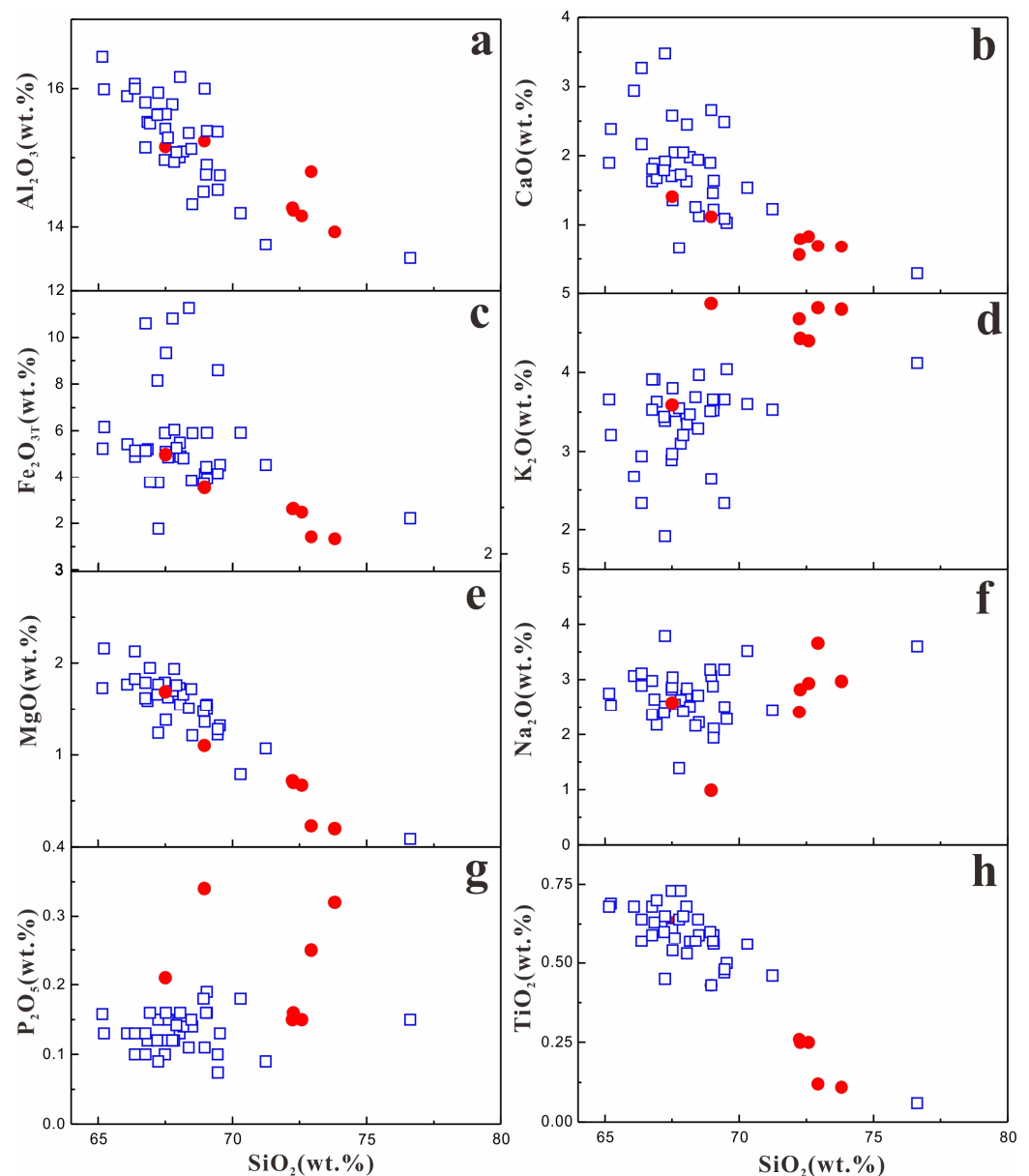


**Figure 5.** Major element Harker diagrams for Jiningian granodiorite in Dahutang deposit. (a)  $\text{Al}_2\text{O}_3$  vs.  $\text{SiO}_2$ ; (b)  $\text{CaO}$  vs.  $\text{SiO}_2$ ; (c)  $\text{Fe}_2\text{O}_3\text{T}$  vs.  $\text{SiO}_2$ ; (d)  $\text{K}_2\text{O}$  vs.  $\text{SiO}_2$ ; (e)  $\text{MgO}$  vs.  $\text{SiO}_2$ ; (f)  $\text{Na}_2\text{O}$  vs.  $\text{SiO}_2$ ; (g)  $\text{P}_2\text{O}_5$  vs.  $\text{SiO}_2$ ; (h)  $\text{TiO}_2$  vs.  $\text{SiO}_2$ . Previous data from [20,21,38,39], as shown in Table S2.

#### 4.2. Zircon Chronology and Trace Elements

In the CL diagram, most zircon grains are greyish white, long columnar, about 150 to 250  $\mu\text{m}$  long, with a length/width ratio of about 1:3. However, the Th/U ratio of zircons ranges from 0.12 to 2.06, plenty of which are less than 0.4 (Figure 6), indicating that these zircons are not of typical magmatic origin [41]. Some zircons have oscillatory zonation inside but dark rims as well, especially zircons in granodiorite samples 17SWD-5, 17SWD-6 (Figure 7). The upper intersection ages of the zircon samples 17SWD-1, 17SWD-2 are  $845 \pm 21$  Ma (MSWD = 1.7) and  $828.7 \pm 7.5$  Ma (MSWD = 1.0), respectively (Figure 8). Harmonic plots were not plotted as the data points for some samples of 17SWD-5 and 17SWD-6 (such as 17SWD-5-2, 17SWD-6-3, 17SWD-6-15 in Figure 7) deviated from the U-Pb harmonic line. Zircon U-Pb dating results are presented in Supplementary Table S3.

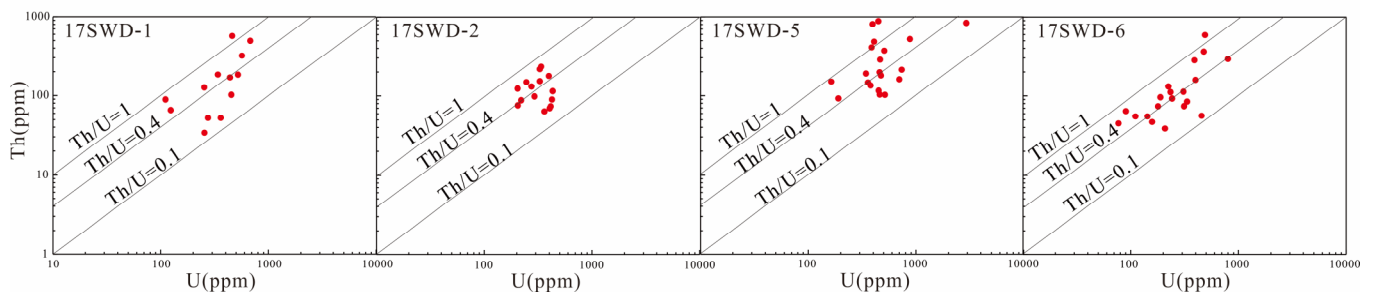


**Figure 6.** Th, U content and Th/U ratio of different zircon samples in the Dahutang deposit.

The zircons in the Jiningian granodiorite have a total rare earth element content of 339.56 to 4415.60 ppm, with an average of 1863.61 ppm.  $\Sigma$ LREE ranges from 2.46 ppm to 2205.42 ppm, and  $\Sigma$ HREE ranges from 337.10 to 3719.67 ppm, which is characterized by an enrichment of heavy rare earths with the exception of some samples with a high content of light rare earths. In addition, our zircon samples have moderate to strong negative Eu anomalies ( $Eu^* = 0.01\text{--}0.57$ ) and intense positive Ce anomalies ( $Ce^* = 0.99\text{--}97.72$ ). Detailed zircon trace elements data are shown in Supplementary Table S4.

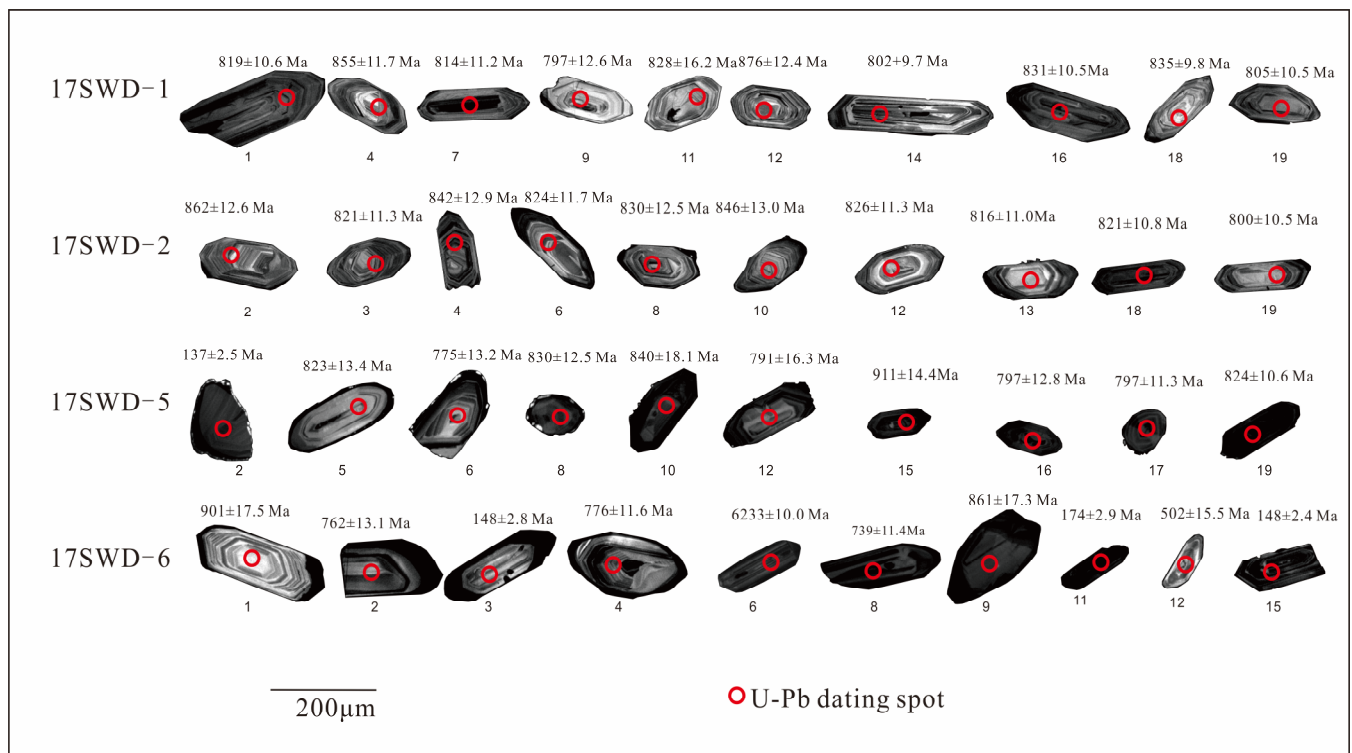


**Figure 7.** Representative CL images of Dahutang deposit zircons. Shown are the apparent  $^{206}\text{Pb}/^{238}\text{U}$  ages with a  $1\sigma$  confidence interval; values under each grain correspond to analytical data in Table S3, and the concordance of each spot is noted in the same table.

## 5. Discussion

### 5.1. Zircon Geochemistry

Zircon is a geochemically stable accessory mineral with a high U-Pb closure temperature [41,42]. However, zircons are susceptible to alteration under fluid interaction, bringing “hydrothermal mineral” characteristics to the original zircons, called “hydrothermal zircon” [43–47]. Hydrothermal fluids account for zircon edges, resulting in the rounding of zircon grain edges or the appearance of other corrosion structures and altering the trace

element characteristics of zircon. Moreover, the formation of the wide alteration edge and the reset of zircon U-Pb systems can also be caused by hydrothermal alteration [48,49].

The zircon U-Pb dating results for the Jiningian granodiorite samples (17SWD-1, 17SWD-2) are  $845 \pm 21$  Ma (MSWD = 1.7) and  $828.7 \pm 7.5$  Ma (MSWD = 1.0), respectively (Figure 8). The result agrees with the previous dating results within the margin of error (819 Ma, [20]), representing the formation time of the Jiningian granodiorite. However, we noticed that some zircon grains have corrosion structures and accretionary edges, which are the characteristics of hydrothermal zircons (Figure 6). Among them, there are three zircons with  $^{206}\text{Pb}/^{238}\text{U}$  ages of  $137 \pm 2.5$  Ma,  $148 \pm 2.8$  Ma and  $148 \pm 2.7$  Ma (17SWD-5-2, 17SWD-6-3 and 17SWD-6-15 in Figure 7), which are more consistent with the age of Yanshanian orogenic hydrothermal activity (150–139 Ma, [3,5,7–14]). Hydrothermal zircons usually have a high content of rare earth elements (especially light rare earth elements) and possess low  $(\text{Sm}/\text{La})_{\text{N}}$  ratio and Ce positive anomaly values [50–52]. The  $(\text{Sm}/\text{La})_{\text{N}}$  vs.  $\delta\text{Ce}$  (Figure 9a) and La vs.  $(\text{Sm}/\text{La})_{\text{N}}$  (Figure 9b) diagrams suggest that zircons in Jiningian granodiorite are influenced by hydrothermal fluids to different degrees. In Figure 10, the zircon REE patterns are not uniform, and parts of them are similar to typical hydrothermal zircons, especially the enrichment of LREEs, which implies heterogeneity in the hydrothermal alteration of zircons.

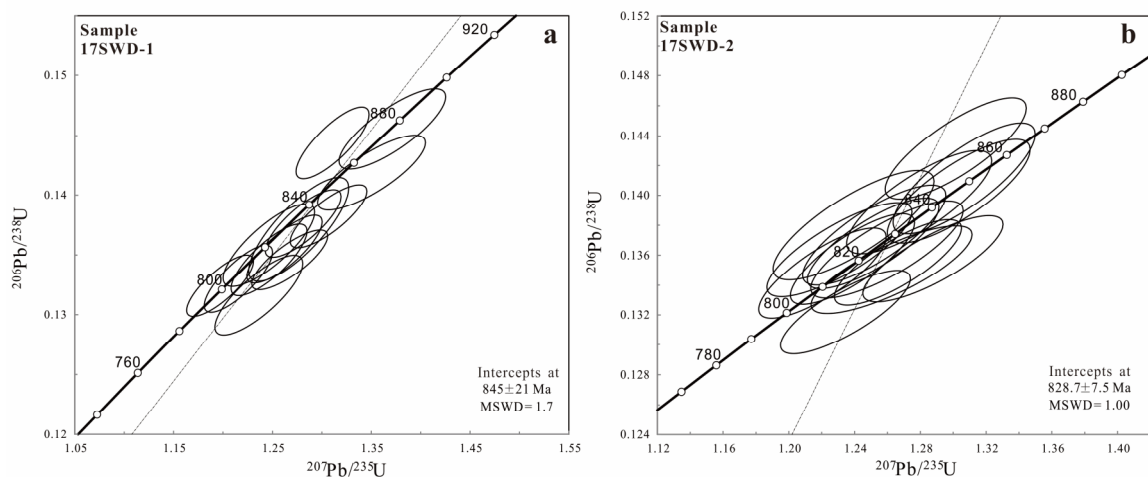


**Figure 8.** U-Pb concordance diagram of zircons from Jiningian granodiorite (a) Sample 17SWD-1 and (b) Sample 17SWD-2.

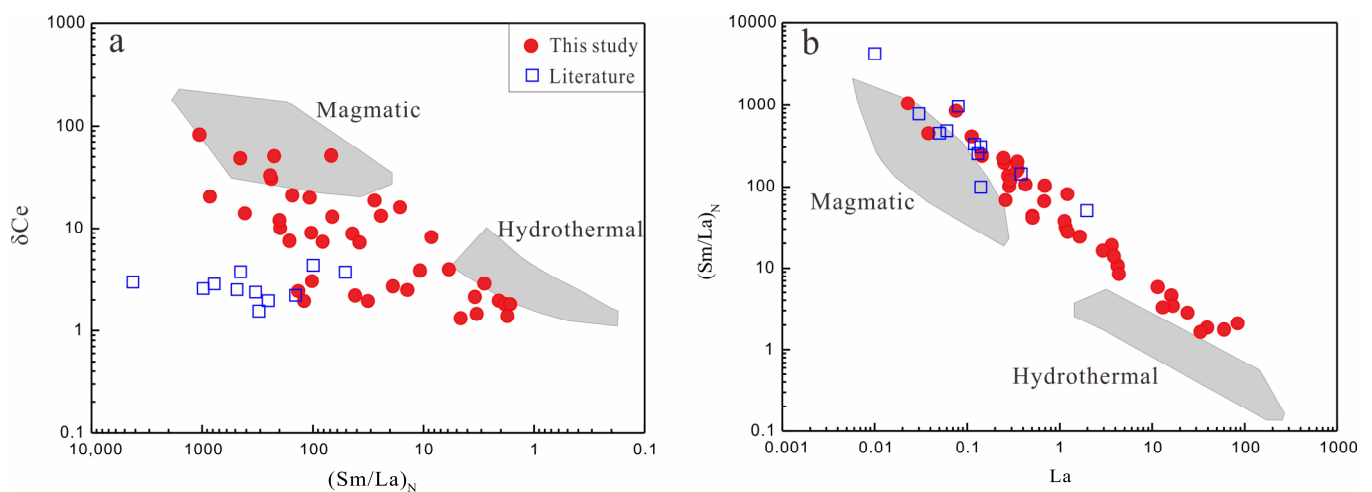


**Figure 9.** Zircon genetic discriminant diagrams for the Dahutang deposit (Modified after [47]). Previous data from [9]. (a)  $(\text{Sm}/\text{La})_{\text{N}}$  vs.  $\delta\text{Ce}$  and (b) La vs.  $(\text{Sm}/\text{La})_{\text{N}}$ .

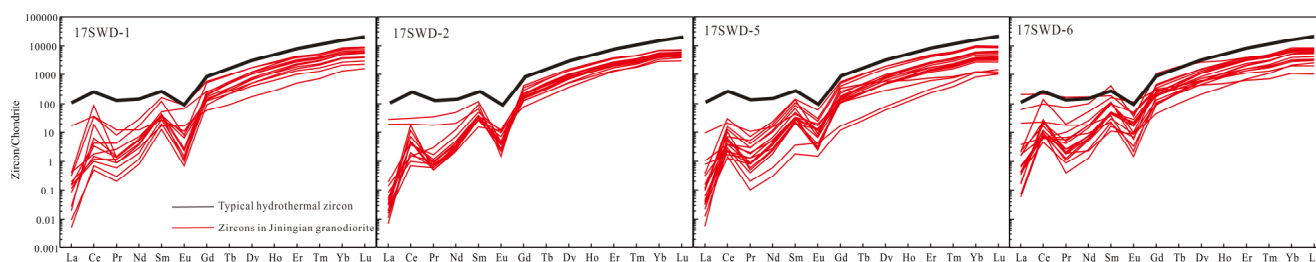


**Figure 10.** Chondrite-normalized REE patterns for different zircon samples in the Dahutang deposit. Chondrite values are from [53], and typical zircon is from [47].

Based on the CL images, REE patterns, U-Pb age and trace elements discriminatory charts, the presence of hydrothermal zircons can be confirmed. Hydrothermal zircons can record the age of hydrothermal activity [45,48]. In our study, the firstly discovered ~140 Ma hydrothermal zircons, whose age is more consistent with the age of mineralization (150–139 Ma [3,5,7–14]), imply a strong superimposed modification of the Jiningian rocks by mineralizing fluids during the Yanshanian mineralization event. Additionally, they verify the view that the Jiningian pluton provides part of the W [9,22,54]. Moreover, zircons in the Jiningian rocks previously studied show typical magmatic zircon characteristics (Figure 9). The difference between them and ours is that our samples are closer to the ore body, which confirms that the overlay renovation of the Jiningian pluton is caused by Yanshanian mineralizing fluids.

### 5.2. Whole Rock Geochemistry

The Jiningian granodiorite in the Dahutang deposit is part of the famous Jiuling batholith, which is the most extensive Neoproterozoic granitoid intrusion in South China [21]. Previous studies have revealed that the Ca content of the Yanshanian rocks is too low for large-scale scheelite mineralization, and the large-scale, Ca-rich Jiningian rocks solve this problem precisely [7,19,20]. However, based on the high W content of the Jiningian rocks (93 ppm on average), it is difficult to deny their contribution to the mineralized material, which has often been overlooked by previous scholars.

In the TAS diagram (Figure 3) and Harker diagrams (Figure 5), the granodiorite in this study and the previous samples belong to the Jiuling Jiningian batholith. Moreover, the near-mineralized Jiuling granodiorite we firstly discovered with SiO<sub>2</sub> content between 72.27% and 73.81% fills a gap in previous studies. SiO<sub>2</sub> and P<sub>2</sub>O<sub>5</sub> are positively correlated, which is an important feature of S-type granite [55]. In the A/CNK diagram (Figure 4), our samples not only have peraluminous characteristics but also fall in the range of A/CNK greater than 1.1, as studied before, which also display S-type granite features. In addition, the differentiation index (DI) of the Jiningian granodiorite averages 89 (Table S1), suggesting that the granite has undergone a high degree of segregation and crystallization. Highly differentiated S-type granites are closely associated with the formation of tungsten deposits [1,4,18]. These characteristics of the Jiningian granodiorite indicate that it has a high W mineralization potential. Moreover, the trace element W contents of our samples amount up to 93 ppm, which has also been reported previously (27 ppm, [16]), indicating that the Jiningian granodiorite is able to provide mineralized material in Yanshanian metallogenic events.

### 5.3. Ore formation Mechanisms and Models

For massive development of fine-vein dipping scheelite in the Jiningian granodiorite, two conditions must be met: firstly, sufficient tungsten in the mineralizing fluid and, secondly, a large amount of calcium in the fluid [6]. For the source of the mineralizing fluid, evidence from hydrogen, oxygen isotopes of H<sub>2</sub>O in fluid inclusion and wolframite oxygen isotopes reveal that it is derived from Yanshanian magma, and trace element studies of scheelite prove the addition of Jiningian granodiorite in the late evolution of

mineralizing fluids [56,57]. The development of many alteration types such as the potassic and sodic alteration in our samples (Figure 2), together with the firstly reported Yanshanian hydrothermal zircons, verifies the strong material exchange between the mineralizing fluids and Jiningian granodiorite. Under the influence of Yanshanian hydrothermal fluids, the calcium-rich plagioclase in the Jiningian pluton de-composed, releasing large amounts of  $\text{Ca}^{2+}$  into the hydrothermal fluids and taking part in the formation of scheelite [7]. In this process, part of the W in the Jiningian pluton is also released into the hydrothermal fluid, which can be proven by the positive correlation of W and Ca in Jiningian granodiorite (Figure 11a). However, the disintegration of plagioclase does not result in the release of W into the fluid. According to the study before, the alkaline account, such as K-feldspathization and albitization, can further activate the transfer of tungsten, which is important for tungsten mineralization, while rocks with alkali feldsparization show depletion of W [15]. There is a wide range of variation in the W content of our samples (13–172 ppm, Table S1), the depletion of W in part of our samples may result from the alkali feldsparization. The significant negative correlation between Na and W and no correlation between K and W (Figure 11b,c) indicates that albitization is the major mechanism of releasing W [57].

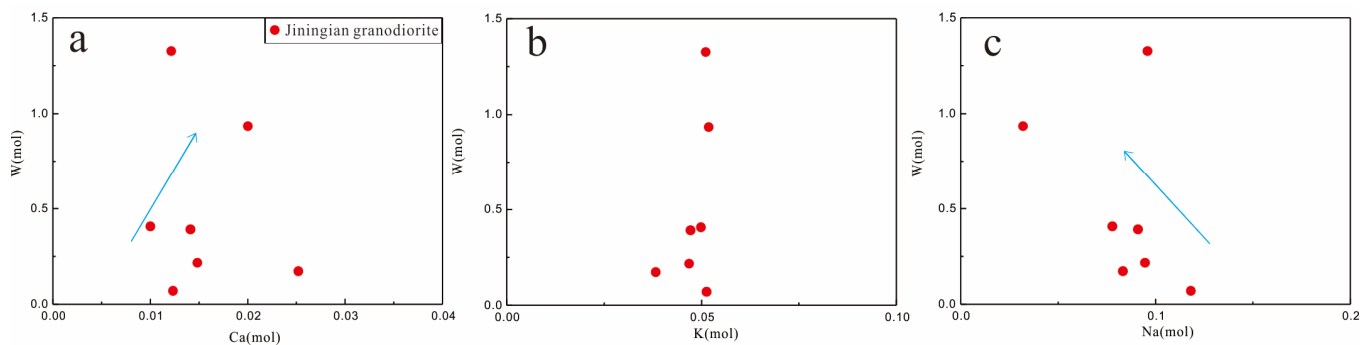


**Figure 11.** Ca-W, K-W and Na-W correlation diagram. The molarity of Ca, K and Na is obtained by dividing the major and trace elements ( $\text{CaO}$ ,  $\text{K}_2\text{O}$ ,  $\text{Na}_2\text{O}$  and W) by their respective relative molecular or atomic masses. (a) Ca vs. W, (b) K vs. W and (c) Na vs. W. The blue arrow indicates the trend of correlation.

Based on our research and combined with previous results, we propose a mineralization model for porphyry scheelite in the Dahutang deposit (Figure 12). In the context of Yanshanian lithosphere stretches after a strong squeeze, granite and mudstone in the Precambrian basement underwent remelting to form granitic magmas. [3,9] With the intrusion of Yanshanian magma into the Jiningian rocks, Yanshanian hydrothermal fluids were able to make full contact with the Jiningian pluton and undergo strong water–rock reactions. Under the action of hydrothermal fluids, the calcium-rich plagioclase in the Jiningian pluton decomposed, releasing a large amount of calcium into the hydrothermal fluids to participate in the formation of scheelite. During this period, sodic feldspathic alteration by hydrothermal action caused activation and release of W in the Jiningian pluton [58], which allows the Jiningian pluton with high W content to provide part of the tungsten element for mineralization.

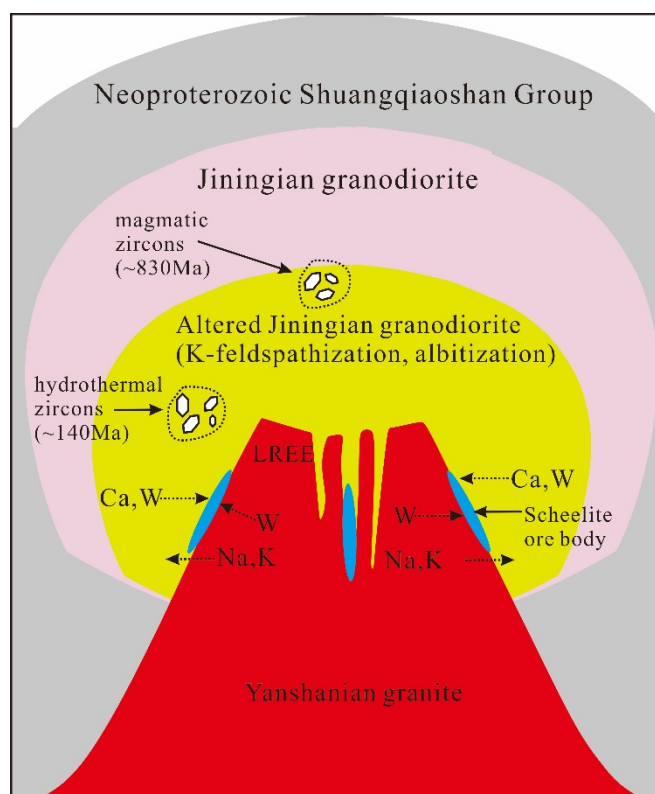


**Figure 12.** Mineralization model for porphyry scheelite in the Dahutang deposit (modified after [58]).

## 6. Conclusions

(1) The U-Pb age of the Jiningian granodiorite samples (17SWD-1, 17SWD-2) are  $845 \pm 21$  Ma (MSWD = 1.7) and  $828.7 \pm 7.5$  Ma (MSWD = 1.0), respectively, which can represent the formation age of Jiningian pluton.

(2) The discovery of the Yanshanian hydrothermal zircons (~140 Ma) proves that the Jiningian pluton was strongly modified by the Yanshanian hydrothermal fluids.

(3) In the ore-forming process, the Jiningian pluton acts as a source of calcium while also providing part of the W. Albitization is the main controlling factor for this procedure in the alkaline account.

**Supplementary Materials:** The following supporting information can be downloaded at: [www.mdpi.com/article/10.3390/min12040428/s1](http://www.mdpi.com/article/10.3390/min12040428/s1), Table S1. Major elements (wt%) and trace elements ( $\mu\text{g/g}$ ) in Dahutang granodiorite, Table S2. Previous major elements (wt%) and trace elements ( $\mu\text{g/g}$ ) in Dahutang granodiorite, Table S3. LA-ICP-MS zircon U-Pb isotopic dating of Dahutang granodiorite, Table S4. Trace element composition of zircons (in ppm) for granodiorite from the Dahutang deposit.

**Author Contributions:** Conceptualization, G.X., Z.L., X.Y. and L.L.; data curation, G.X., Z.L. and X.Y.; formal analysis, G.X., Z.L., X.Y. and L.L.; funding acquisition, G.X., X.Y. and L.L.; investigation, G.X., X.Y. and L.L.; methodology, G.X., X.Y. and L.L.; project administration, X.Y. and L.L.; resources, X.Y. and L.L.; software, L.L.; supervision, X.Y.; visualization, G.X. and Z.L.; writing—original draft, G.X. and Z.L.; writing—review & editing, G.X., Z.L., X.Y. and L.L. All authors have read and agreed to the published version of the manuscript.

**Funding:** The study is supported by MOST of China (No. 2016YFC0600404), the National Key Research and Development Program of China (2018YFC0603901) and the Natural Science Foundation of China (41972198).

**Data Availability Statement:** Not Applicable.

**Acknowledgments:** Three reviewers and editors are much appreciated for their constructive comments.

**Conflicts of Interest:** The authors declare no conflicts of interest.

## References

1. Chen, J.; Lu, J.J.; Chen, W.F.; Wang, R.C.; Ma, D.S.; Zhu, J.C.; Zhang, W.L.; Ji, J.F. W-Sn-Nb-Ta-Bearing granites in the nanling range and their relationship to metallogenesis. *Geol. J. China Univ.* **2008**, *14*, 459–473. (In Chinese with English Abstract)
2. Ma, D.S. Progress in Research on geochemistry of Tungsten. *Geol. J. China Univ.* **2009**, *15*, 19–34. (In Chinese with English Abstract)
3. Mao, Z.H.; Cheng, Y.B.; Liu, J.J.; Yuan, S.D.; Wu, S.H.; Xiang, X.K.; Luo, X.H. Geology and molybdenite Re-Os age of the Dahutang granite-related veinlets-disseminated tungsten ore field in the Jiangxin Province, China. *Ore Geol. Rev.* **2013**, *53*, 422–433.
4. Mao, J.W.; Wu, S.H.; Song, S.W.; Dai, P.; Xie, G.Q.; Su, Q.W.; Liu, P.; Wang, X.G.; Xu, Z.Z.; Chen, X.Y.; et al. The world-class Jiangnan tungsten belt: Geological characteristics, metallogeny, and ore deposit model. *Chin. Sci. Bull.* **2020**, *65*, 3746–3762. (In Chinese with English Abstract)
5. Mao, Z.H.; Liu, J.J.; Mao, J.W.; Deng, J.; Zhang, F.; Meng, X.Y.; Xiong, B.K.; Xiang, X.K.; Luo, X.H. Geochronology and geochemistry of granitoids related to the giant Dahutang tungsten deposit, middle Yangtze River region, China: Implications for petrogenesis, geodynamic setting, and mineralization. *Gondwana Res.* **2015**, *28*, 816–836.
6. Xiang, X.K.; Wang, P.; Zhan, G.N.; Sun, D.M.; Zhong, B.; Qian, Z.Y.; Tan, R. Geological characteristics of Shimensi tungsten polymetallic deposit in northern Jiangxi Province. *Miner. Depos.* **2013**, *32*, 1171–1187. (In Chinese with English Abstract)
7. Fan, X.K. *Study on Metallogenic Mechanism of the Giant Dahutang Tungsten Polymetallic Orefield in Jiangxi Province*; Chinese Academy of Geological Sciences: Beijing, China, 2019; 206p. (In Chinese with English Abstract)
8. Huang, L.C.; Jiang, S.Y. Geochronology, geochemistry and petrogenesis of the tungsten-bearing porphyritic granite in the Dahutang tungsten deposit, Jiangxi Province. *Acta Petrol. Sin.* **2013**, *29*, 4323–4335. (In Chinese with English Abstract)
9. Li, H.W.; Zhao, Z.; Chen, Z.Y.; Guo, N.X.; Gan, J.W.; Li, X.W.; Yin, Z. Genetic relationship between the two-period magmatism and W mineralization in the Dahutang ore-field, Jiangxi Province: Evidence from zircon geochemistry. *Acta Petrol. Sin.* **2021**, *37*, 1508–1530. (In Chinese with English Abstract)
10. Lin, L.; Zhan, G.L.; Yu, X.P. Geological characteristics and ore-search prospect of Dahutang tungsten(tin) orefield in Jiangxi. *Resour. Surv. Environ.* **2006**, *27*, 25–32. (In Chinese with English Abstract)
11. Pan, D.P.; Wang, D.; Wang, X.L. Petrogenesis of granites in Shimensi in northwestern Jiangxi Province and its implications for tungsten deposits. *Geol. China.* **2017**, *44*, 118–135. (In Chinese with English Abstract)
12. Xiang, X.K.; Wang, P.; Sun, D.M.; Zhong, B. Re-Os isotopic age of molybdenite from the Shimensi tungsten polymetallic deposit in northern Jiangxi province and its geological implications. *Geol. Bull. China.* **2013**, *32*, 1824–1831. (In Chinese with English Abstract)
13. Xiang, X.K.; Yin, Q.Q.; Sun, K.K.; Chen, B. Origin of the Dahutang syn-collisional granite-porphyry in the middle segment of the Jiangnan orogen: Zircon U-Pb geochronologic, geochemical and Nd-Hf isotopic constraints. *Acta Petrol. Mineral.* **2015**, *34*, 581–600. (In Chinese with English Abstract)
14. Ye, H.M.; Zhang, X.; Zhu, Y.H. In-situ Monazite U-Pb Geochronology of Granites in Shimensi Tungsten Polymetallic Deposit, Jiangxi Province and its Geological Significance. *Geotecton. Metallog.* **2016**, *40*, 58–70. (In Chinese with English Abstract)
15. Liu, Y.J. Discussion on the geospheroidization of tungsten ore formation. *Geol. Explor.* **1982**, *1*, 17–25. (In Chinese with English Abstract)
16. Zuo, Q.S. Analysis on the geologic conditions and the assessment of the further ore-finding foreground from Dahutang to Liyangdou metallogenic region in the western part of Jiulingshan, Jiangxi province. *Resour. Environ. Eng.* **2006**, *20*, 348–353. (In Chinese with English Abstract)
17. Rudnick, R.; Gao, S. Composition of the Continental Crust. *Treatise Geochem.* **2003**, *3*, 1–64.
18. Wu, X.Y.; Zhang, Z.Y.; Zheng, Y.C.; Dai, J.L.; Fan, X.K.; Sheng, Y.C. Magmatism, genesis and significance of multi-stage porphyry-like granite in the giant Dahutang tungsten deposit, northern Jiangxi Province. *Acta Petrol. Mineral.* **2019**, *38*, 318–338. (In Chinese with English Abstract)
19. Jiang, S.Y.; Peng, N.J.; Huang, L.C.; Xu, Y.M.; Zhan, G.L.; Dan, X.H. Geological characteristic and ore genesis of the giant tungsten deposits from the Dahutang ore-concentrated district in northern Jiangxi Province. *Acta Petrol. Sin.* **2015**, *31*, 639–655. (In Chinese with English Abstract)
20. Sun, K.K.; Chen, B.; Chen, J.S.; Xiang, X.K. The petrogenesis of the Jiuling granodiorite from the Dahutang deposit, Jiangxi Province and its tectonic implications. *Acta Petrol. Sin.* **2017**, *33*, 907–924. (In Chinese with English Abstract)
21. Li, X.H.; Li, Z.X.; Ge, W.C.; Zhou, H.W.; Li, W.X.; Liu, Y.; Wingate, M.T.D. Neoproterozoic granitoids in South China: Crustal melting above a mantle plume at ca. 825 Ma? *Precambrian Res.* **2003**, *122*, 45–83.
22. Song, W.L.; Yao, J.M.; Chen, H.Y.; Sun, W.D.; Lai, C.K.; Xiang, X.K.; Luo, X.H.; Jourdan, F. A 20 m.y. long-lived successive mineralization in the giant Dahutang W-Cu-Mo deposit, South China. *Ore Geol. Rev.* **2018**, *95*, 401–407.
23. Chang, Y.F.; Liu, X.P.; Wu, C.Y. *The Copper-Iron Belt of the Lower and Middle Reaches of the Changjiang River*. Geological Publishing House Press: Beijing, China, 1991; pp. 1–234. (In Chinese with English Abstract)

24. Mao, J.W.; Xiong, B.K.; Liu, J.; Pirajno, F.; Cheng, Y.B.; Ye, H.S.; Song, S.W.; Dai, P. Molybdenite Re/Os dating, zircon U-Pb age and geochemistry of granitoids in the Yangchuling porphyry W-Mo deposit (Jiangnan tungsten ore belt), China: Implications for petrogenesis, mineralization and geodynamic setting. *Lithos* **2017**, *286*, 35–52.
25. Wang, X.L.; Zhou, J.C.; Griffin, W.L.; Zhao, G.C.; Yu, J.H.; Qiu, J.S.; Zhang, Y.J.; Xing, G.F. Geochemical zonation across a Neoproterozoic orogenic belt: Isotopic evidence from granitoids and metasedimentary rocks of the Jiangnan orogen, China. *Precambrian Res.* **2014**, *242*, 154–171.
26. Gao, L.Z.; Liu, Y.X.; Wang, M.; Wang, X.H.; Chen, J.S.; Ding, X.Z.; Zhang, C.H.; Cao, Q. Zircon SHRIMP U-Pb dating of tuff bed of the Sibao Group in southeastern Guizhou-northern Guangxi area, China and its stratigraphic implication. *Geol. Bull. China*, **2010**, *29*, 1259–1267. (In Chinese with English Abstract)
27. Zhao, J.H.; Zhou, M.F.; Yan, D.P.; Zheng, J.P.; Li, J.W. Reappraisal of the ages of Neoproterozoic strata in South China: No connection with the Grenvillian orogeny. *Geology* **2011**, *39*, 299–302.
28. Gao, L.Z.; Yang, M.G.; Ding, X.Z.; Liu, Y.X.; Liu, X.; Ling, L.H.; Zhang, C.H. SHRIMP U-Pb zircon dating of tuff in the Shuangqiaoshan and Heshangzhen groups in South China—constraints on the evolution of the Jiangnan Neoproterozoic orogenic belt. *Geol. Bull. China*, **2008**, *27*, 1744–1751. (In Chinese with English Abstract)
29. Gilder, S.A.; Keller, G.R.; Luo, M.; Goodell, P.C. Eastern Asia and the Western Pacific timing and spatial distribution of rifting in China. *Tectonophysics* **1991**, *197*, 225–243.
30. Zhou, X.M.; Li, W.X. Origin of Late Mesozoic igneous rocks in Southeastern China: Implications for lithosphere subduction and underplating of mafic magmas. *Tectonophysics* **2000**, *326*, 269–287.
31. Han, L.; Huang, X.L.; Li, J.; He, P.L.; Yao, J.M. Oxygen fugacity variation recorded in apatite of the granite in the Dahutang tungsten deposit, Jiangxi Province, South China. *Acta Petrolo. Sin.* **2016**, *32*, 746–758. (In Chinese with English Abstract)
32. Feng, C.Y.; Wang, H.; Xiang, X.K.; Zhang, M.Y. Late Mesozoic granite-related W-Sn mineralization in the northern Jiangxi region, SE China: A review. *J. Geochem. Explor.* **2018**, *195*, 31–48.
33. Feng, C.Y.; Zhang, D.Q.; Xiang, X.K.; Li, D.X.; Qu, H.Y.; Liu, J.N.; Xiao, Y. Re-Os isotopic dating of molybdenite from the Dahutang tungsten deposit in northwestern Jiangxi Province and its geological implication. *Acta Petrol. Sin.* **2012**, *28*, 3858–3868. (In Chinese with English Abstract)
34. Achterberg, V.E.; Ryan, C.G.; Jackson, S.E.; Griffin, W.L. Data reduction software for LA-ICP-MS. In *Laser-Ablation-ICPMS in the Earth Sciences. Principles and Applications*; Sylvester, P.J., Ed.; Mineralogical Society of Canada Short Course Series 29; Mineralogical Society of Canada: Quebec City, QC, Canada, 2001.
35. Li, Y.G.; Wang, S.S.; Liu, M.W.; Meng, E.; Wei, X.Y.; Zhao, H.B.; Qi, M.Q. U-Pb Dating Study of Baddeleyite by LA-ICP-MS: Technique and Application. *Acta Geol. Sin.* **2015**, *89*, 2400–2418. (In Chinese with English Abstract)
36. Ludwig, K.R. *User's Manual for Isoplot 3.00. A Geochronological Toolkit for Microsoft Excel*; No. 4a; Special Publication; Berkeley Geochronology Center: Berkeley, CA, USA, 2003.
37. Middlemost, E.; Naming materials in the magma/igneous rock system. *Earth-Sci. Rev.* **1994**, *37*, 215–224.
38. Rong, W.; Zhang, S.B.; Zheng, Y.F. Back-reaction of Peritectic Garnet as an Explanation for the Origin of Mafic Enclaves in S-type Granite from the Jiuling Batholith in South China. *J. Petrol.* **2017**, *58*, 569–598.
39. Zhang, F.S.; Xu, J.; Zhang, J.; Guo, J.S. Geochemical characteristics, zircon U-Pb age and geological significance of New Proterozoic granites in Jiuling area, Jiangxi Province. *J. East China Uni. Technol. (Nat. Sci.)* **2020**, *43*, 12–20. (In Chinese with English Abstract)
40. Maniar, P.D.; Piccoli, P.M. Tectonic discrimination of granodiorite. *Geol. Soc. Am. Bull.* **1989**, *101*, 635–643.
41. Wu, Y.B.; Zheng, Y.F. Zircon genetic mineralogy and its constraints on the interpretation of U-Pb age. *Chin. Sci. Bull.* **2004**, *49*, 1589–1604. (In Chinese with English Abstract)
42. Wilde, S.A.; Valley, J.W.; Peck, W.H.; Graham, C.M. Evidence from detrital zircons for the existence of continental crust and oceans on the Earth 4.4 Gyr ago. *Nature* **2001**, *409*, 175–178.
43. Bell, E.A.; Boehnke, P.; Harrison, T.M. Recovering the primary geochemistry of Jack Hills zircons through quantitative estimates of chemical alteration. *Geochim. Cosmochim. Ac.* **2016**, *191*, 187–202.
44. Mueller, A.G.; McNaughton, N.J. Mineral equilibria and zircon, garnet and titanite U-Pb ages constraining the PTt path of granite-related hydrothermal systems at the Big Bell gold deposit, Western Australia. *Miner. Deposita.* **2018**, *53*, 105–126.
45. Zhu, Y.F.; Song, B. Petrology and SHRIMP chronology of mylonitized Tianger granite, Xinjiang: Also about the dating on hydrothermal zircon rim in granite. *Acta Petrol. Sin.* **2006**, *22*, 135–144. (In Chinese with English Abstract)
46. Yang, W.B.; Niu, H.S.; Qiang, S.; Weidong, Z.; Hong, L.; Ning-Bo, J.; Yuhang, Y. Geochemistry of magmatic and hydrothermal zircon from the highly evolved Baerzhe alkaline granite: Implications for Zr-REE-Nb mineralisation. *Miner. Deposita.* **2013**, *49*, 451–470.
47. Wei, T.C.; Mei-Fu, Z. Hydrothermal alteration of magmatic zircon related to NaCl-rich brines: Diffusion-reaction and dissolution-reprecipitation processes. *Amer. J. Sci.* **2017**, *317*, 177–215.
48. Li, C.M. Review on the Mineralogy and Situ Microanalytical Dating Techniques of Zircons. *Geolo. Surv. Res.* **2009**, *32*, 161–174. (In Chinese with English Abstract)
49. Kaulina, T.; Lyalina, L.; Kamenetsky, V.; Il'chenko, V.; Bocharov, V.; Gannibal, M. Composition and Structure of Zircon from Hydrothermal Uranium Occurrences of the Litsa Ore Area (Kola Region, Russia). *Geoscience* **2020**, *10*, 278.
50. Hoskin, P.W.O. Trace-element composition of hydrothermal zircon and the alteration of Hadean zircon from the Jack Hills, Australia. *Geochim. Cosmochim. Ac.* **2005**, *69*, 637–648.

51. Zhao, Z.H. Trace element geochemistry of accessory minerals and its applications in petrogenesis and metallogenesis. *Earth Sci. Front.* **2010**, *17*, 267–286. (In Chinese with English Abstract)
52. Toscano, M.; Pascual, E.; Nesbitt, R.W.; Almodóvar, G.R.; Sáez, R.; Donaire, T. Geochemical discrimination of hydrothermal and igneous zircon in the Iberian Pyrite Belt, Spain. *Ore Geol. Rev.* **2014**, *56*, 301–311.
53. Sun, S.S.; McDonough, W.F. Chemical and isotopic systematics of oceanic basalts: Implications for mantle composition and processes. Magmatism in the Ocean Basalts. *Geol. Soc. Publ.* **1989**, *42*, 313–345.
54. Zhang, Y.; Gao, J.F.; Ma, D.S.; Pan, J.Y. The role of hydrothermal alteration in tungsten mineralization at the Dahutang tungsten deposit, South China. *Ore Geol. Rev.* **2018**, *95*, 1008–1027.
55. Li, X.H.; Li, W.X.; Li, Z.X. A further discussion of the genetic type and tectonic significance of the early Yanshanian granites of the Nanling Ridge. *Chin. Sci. Bull.* **2007**, *52*, 981–991. (In Chinese with English Abstract)
56. Chen, C.F.; Gao, J.F.; Zhang, Q.Q.; Min, K. Evolution of ore-forming fluids in Shimensi tungsten polymetallic deposit of northern Jiangxi: Constraints from in situ trace element analysis of scheelite. *Miner. Depos.* **2021**, *40*, 293–310. (In Chinese with English Abstract)
57. Wang, H.; Feng, C.Y.; Li, D.X.; Xiang, X.K.; Zhou, J.H. Sources of granitoids and ore-forming materials of Dahutang tungsten deposit in northern Jiangxi Province: Constraints from mineralogy and isotopic tracing. *Acta. Petrol. Sin.* **2015**, *31*, 725–739.
58. Zhao, H.B.; Zhang, Y.; Liu, L. Hydrothermal alteration processes in the giant Dahutang tungsten deposit, South China: Implications from litho-geochemistry and mass balance calculation. *China Geol.* **2021**, *4*, 230–244.